Two-dimensional silicon photonic crystal based biosensing platform for protein detection

Mindy Lee* **and Philippe M. Fauchet**

The Institute of Optics, [2]Department of Electrical and Computer Engineering, University of Rochester
Rochester, New York 14627
*mindylee@optics.rochester.edu

Abstract: We theoretically and experimentally demonstrate an ultra-sensitive two-dimensional photonic crystal microcavity biosensor. The device is fabricated on a silicon-on-insulator wafer and operates near its resonance at 1.58 μm. Coating the sensor internal surface with proteins of different sizes produces a different amount of resonance redshift. The present device can detect a molecule monolayer with a total mass as small as 2.5 fg. The device performance is verified by measuring the redshift corresponding to the binding of glutaraldehyde and bovine serum albumin (BSA). The experimental results are in good agreement with theory and with ellipsometric measurements performed on a flat oxidized silicon wafer surface.

OCIS codes: (170.4580) Optical diagnostics for medicine; (230.5750) Resonators

References

1. B. Liedberg, I. Lundstrom, and E. Stenberg, "Principles of biosensing with an extended coupling matrix and surface plasmon resonance," Sens. Actuators B **11**, 63-72 (1993).
2. J. J. Saarinen, S. M. Weiss, P. M. Fauchet, and J. E. Sipe, "Optical sensor based on resonant porous silicon structures," Opt. Express **13**, 3754-3764 (2005).
3. V. S.-Y. Lin, K. Motesharei, K. Motesharei, K.-P. S. Dancil, M. J. Sailor, and M. R. Ghadir, "A porous silicon-based optical interferometric biosensor," Science **278**, 840-843 (1997).
4. F. Cunin, T. A. Schmedake, J. R. Link, Y. Y. Li, J. Koh, S. N. Bhatia and M. J. Sailor, "Biomolecular screening with encoded porous-silicon photonic crystals," Nat. Mater. **1**, 39-41 (2002).
5. S. Chan, P. M. Fauchet, Y. Li, L. J. Rothberg, and B. L. Miller, "Porous silicon microcavities for biosensing applications," Phys. Stat. Sol. A. **182**, 541-546 (2000).
6. S. Chan, S. R. Horner, P. M. Fauchet, and B. L. Miller, "Identification of gram negative bacteria using nanoscale silicon microcavities," J. Am. Chem. Soc. **123**, 11797-11798 (2001).
7. H. Ouyang, M. Christophersen, R. Viard, B. L. Miller and P. M. Fauchet, "Macroporous silicon microcavity for macromolecule detection," Adv. Funct. Mater. **15**, 1851-1859 (2005).
8. B. T. Cunningham, P. Li, B. Lin, and J. Pepper, "Colorimetric resonant reflection as a direct biochemical assay technique," Sens. Actuators B **81**, 316-328 (2002).
9. I. D. Block, L. L. Chan and B. T. Cunningham, "Photonic crystal optical biosensor incorporating structured low-index porous dielectric," Sens. Actuators B **120**, 187-193 (2006).
10. G. J. Sonek, "Integrated photonic crystal waveguides for micro-bioanalytical devices" in *Proceedings of IEEE Conference on Microtechnologies in Medicine and Biology* (IEEE, 2005), pp. 333-335.
11. K. Srinivasan and O. Painter, "Momentum space design of high-Q photonic crystal optical cavities," Opt. Express **10**, 670-684 (2002).
12. Y. Akahane, T. Asano, B. Song, and S. Noda, "High-Q photonic nanocavity in a two-dimensional photonic crystal," Nature **425**, 944-947 (2003).
13. B. Schmidt, V. Almeida, C. Manolatou, S. Preble, and M. Lipson, "Nanocavity in a silicon waveguide for ultrasensitive nanoparticle detection," Appl. Phys. Lett. **85**, 4854-4856 (2004).
14. E. Chow, A. Grot, L. W. Mirkarimi, M. Sigalas, and G. Girolami, "Ultracompact biochemical sensor built with two-dimensional photonic crystal microcavity," Opt. Lett. **29**, 1093-1095 (2004).
15. H. Chen, K. K. Tsia and A. W. Poon, "Surface modes in two-dimensional photonic crystal slabs with a flat dielectric margin," Opt. Express **14**, 7368-7377 (2006).
16. O. Painter, J. Vuckovic, and A. Scherer, "Defect modes of a two-dimensional photonic crystal in an optically thin dielectric slab," J. Opt. Am. B **16**, 275-285 (1999).

#79144 - $15.00 USD Received 18 Jan 2007; revised 23 Mar 2007; accepted 23 Mar 2007; published 3 Apr 2007

17. I. D. Kuntz and W. Kauzmann, "Hydration of proteins and polypeptides," Adv. Protein Chem. **28**, 239-345 (1974).
18. P. G. Squire, P. Moser, and C. T. O'Konski, "Hydrodynamic properties of bovine serum albumin monomer and dimer," J. Biochem. **7**, 4261-4272 (1968).
19. H. Ouyang, C. C. Striemer, and P. M. Fauchet, "Quantitative analysis of the sensitivity of porous silicon optical biosensors," Appl. Phys. Lett. **88**, 163108 (2006).
20. V. Kanda, J. K. Kariuki, D. J. Harrison and M. T. McDermott, "Label-Free Reading of Microarray-Based Immunoassays with Surface Plasmon Resonance Imaging," Anal. Chem. **76**, 7257-7262 (2004).
21. D. Nedelkov, K. A. Tubbs and R. W. Nelson, "Surface plasmon resonance-enabled mass spectrometry arrays," Electrophoresis **27**, 3671 (2006).

Early detection and identification of biological substances are pursued with great interest for many applications. Label-free optical biosensing is one of the fastest growing research areas [1-9], because it does not require the use of radioactive / fluorescent labels that introduce complexity and potential contamination to biological material in vivo. The well developed label-free platforms include surface plasmon resonance (SPR) [1], waveguides [2], one-dimensional photonic bandgap structures of increasing complexity, ranging from simple Bragg reflectors [3] and rugate filters [4] to microcavities [5-7] built with porous silicon, and colorimetric imaging obtained from off-plane illumination on a diffractive grating surface / photonic crystal [8-10]. One common problem is that these structures require a well-collimated readout beam, hence a relatively large sensing area.

Photonic crystals (PCs) are an attractive sensing platform because they provide strong light confinement. Unlike many sensing platforms that utilize the interaction between the small evanescent tail of the electromagnetic field and the analyte, PCs can be designed to localize the electric field in the low refractive index region (*e.g.* air pores), which makes the sensors extremely sensitive to a small refractive index change produced by bio-molecule immobilization on the pore walls. By introducing a point defect into a PC, defect states can be pulled down from the air band or up from the substrate band. The corresponding optical spectrum shows narrow transmission peaks inside the bandgap, whose precise position is determined by the refractive index of the pores. Thus, the presence of molecules inside the pores can be detected by monitoring a small spectral shift, especially if high-Q microcavities, which have been reported both theoretically [11] and experimentally [12], are used. Quasi-1D PC waveguides and two-dimensional PC microcavity sensors have been both theoretically and experimentally demonstrated for detecting nanoparticles [13] and ambient refractive index changes [14,15] respectively. However, protein recognition depends on the surface chemistry, thus, instead of filling up the pores and changing the ambient refractive index, the molecules coat the pore walls. In this paper, we demonstrate a two-dimensional PC microcavity biosensor that is capable of monitoring protein binding on the pore walls and quantitively measuring the protein diameter.

The structure depicted in Fig. 1 consists of a hexagonal array of cylindrical air pores in a 400 nm-thick silicon (Si) slab separated from the Si substrate by 1 μm of SiO_2 to provide a good vertical confinement for the propagation modes. The PC has a lattice constant a of 465 nm and a pore diameter d of 270 nm. The defect is introduced by reducing the center pore diameter to 140 nm. Such a configuration gives rise to a resonance in the bandgap close to 1.58 μm for even (TE-like) modes. Here we are primarily interested in studying the TE-like mode because there is no bandgap for TM-like modes beneath the light cone. Two tapered ridge waveguides are used to couple light in / out the microcavity. They are tapered from 2 μm down to ~ 0.7 μm to match the mode of the microcavity. Light is coupled along the Γ-M direction, because the resonance mode in-plane leakage is mainly in the Γ-M direction and hence the coupling efficiency is higher along this direction [16]. The device is patterned using electron beam lithography.

#79144 - $15.00 USD Received 18 Jan 2007; revised 23 Mar 2007; accepted 23 Mar 2007; published 3 Apr 2007

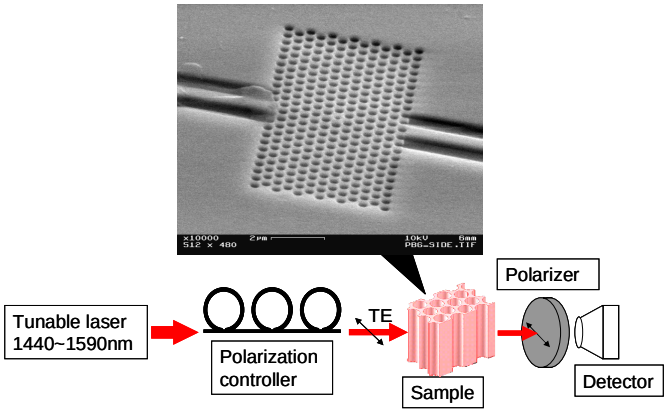

Fig. 1. Scanning electron microscopy photograph of a typical device and schematic of the experimental setup. A tunable laser (1440 nm to 1590 nm) is used as the source. Light is coupled in and out of the PC using tapered ridge waveguides. A polarization controller is used to maximize the TE mode signal, and an InGaAs detector is used to measure the transmission signal.

In our measurement setup, a laser source tunable from 1440 nm to 1590 nm is used. TE polarized light is coupled to a polarization-maintaining tapered lensed fiber and then focused onto the input ridge waveguide. The transmitted signal is coupled out in a similar fashion and measured using an InGaAs detector. To optimize the readout signal to noise ratio, a polarizer controller and a TE polarizer are used before the input and output end respectively. An infrared camera is also used for alignment and monitoring scattering losses.

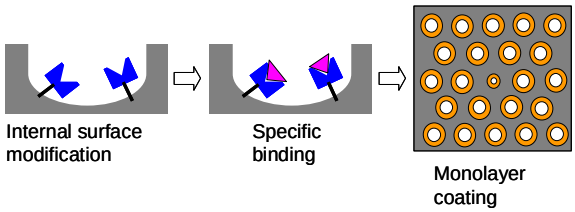

Fig. 2. Schematic of bio-molecule recognition: (a) the target molecules are captured by the probe molecules. (b) The bio-molecules form a uniform layer on the internal surface of the sensor. In reality the layer thickness is very small compared with the pore size.

Figure 2(a) illustrates the bio-molecule binding mechanism. Highly selective probe molecules (ex. DNA, antibody) are immobilized on the internal surface where they form a monolayer and capture the target molecules (ex. DNA, protein). When a probe-functionalized sensor is exposed to the target, a monolayer of target species is again captured on the surface of the sensor. The bio-molecule coating causes a refractive index change only in the vicinity of the pore wall, as shown schematically in Fig. 2(b).

To characterize the sensor performance, we use glutaraldehyde-bovine serum albumin (BSA) binding as the model system because glutaraldehyde has a strong affinity for BSA. The pore size of our device is ~30 times larger than the protein hydrodynamic diameter [17, 18], which guarantees a high infiltration efficiency of the proteins into our device and facilitates the uniform formation of a monolayer-thick coating on the pore walls.

To prepare the surface for the capture of BSA proteins, the device is first thermally oxidized at 800□ to form a silica-like internal surface. The sensor is then treated with 2% amino-propyltrimethoxy-silane to create amino groups on the internal oxide surface, at which point the device is ready for bio-molecule recognition.

#79144 - $15.00 USD Received 18 Jan 2007; revised 23 Mar 2007; accepted 23 Mar 2007; published 3 Apr 2007

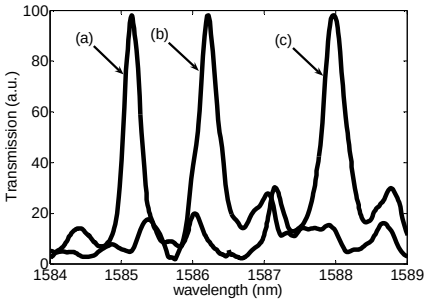

Fig. 3. Normalized transmission spectra of the PC microcavity. Curve (a) indicates the initial spectrum resonance after oxidation and silanization, curve (b) is measured after glutaraldehyde attaches to the pore walls, and curve (c) is obtained after infiltration of BSA molecules.

The transmission spectrum is first measured after oxidation and silanization. Then we use a micro-pipette to apply a 2 μl droplet of 2.5% glutaraldehyde (the probe molecule) on the device, wait until the proteins are immobilized on the pore walls, rinse with de-ionized water and measure the transmission spectrum again. In the end, 2 μl of 2% BSA (the target molecule) is applied. We wait for 30 mins until the two proteins attach completely, rinse away the residue that does not bind and measure the transmission spectrum.

The raw data exhibit Fabry-Perot resonances due to reflection at the waveguide facets and PC edges. These Fabry-Perot resonances are filtered out after performing a fast Fourier transform. Figure 3 shows the smoothed transmission spectra near the microcavity resonance measured at three different binding stages. Curve (a) shows the initial transmission spectrum after oxidation and silanization. Curve (b) is measured after exposure to glutaraldehyde. A resonance redshift of 1.1 nm is observed. Curve (c) shows a redshift of 1.7 nm after BSA binding, thus a total shift of 2.8 nm compared with the initial spectrum.

To model the experimental results, calculations using a finite-domain-time-difference (FDTD) method and a plane-wave expansion with 32 grid points per supercell are performed. In the simulation, the refractive index of the dehydrated proteins is set as 1.45, which is consistent with the literature values [19] and also agrees with an independent ellipsometric measurement that we performed on a flat oxidized silicon wafer.

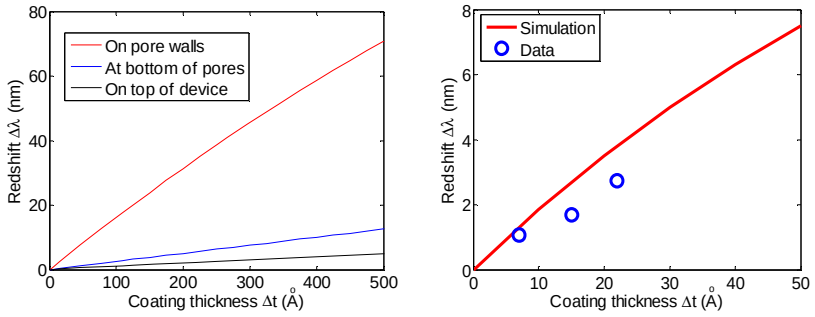

(a) (b)

Fig. 4. (a) Calculated resonance redshift versus the monolayer coating thickness on the pore wall, bottom, and top of the device. (b) Red curve shows the calculated resonance redshift versus the coating thickness on the pore wall. Blue dots show the protein layer thicknesses measured by ellipsometry. The ellipsometric data are in agreement with the model.

In the PC biosensor, the molecules can form a layer everywhere: on the pore walls, at the bottom of the device or on top of the device. 3-D FDTD simulations show that the resonance redshift increases almost linearly with the coating thickness (Fig. 4(a)). The redshift is much

#79144 - $15.00 USD Received 18 Jan 2007; revised 23 Mar 2007; accepted 23 Mar 2007; published 3 Apr 2007

larger when the molecules are attached on the pore walls, whereas the contribution of material on top of the device and at the bottom of the pores is negligible. This is expected because light is mainly confined within the PC slab. By comparing the simulation curve with the experimental shifts shown in Fig. 3, the layers of dehydrated glutaraldehyde and BSA molecules should be 7 Å and 10 Å thick, respectively.

To verify this, we apply the same experimental protocol on a flat oxidized silica wafer and measure the protein thickness using ellipsometry. A thickness of 7±1 Å and 15±5 Å is measured for these two proteins. As shown in Fig. 4(b), the ellipsometric data are in general agreement with the model. We observe a slightly lower resonance shift than predicted, which may result from either an incomplete surface coverage by BSA or an over estimation of the thickness of a BSA monolayer from our preliminary ellipsometric measurement. Future experiments will resolve this issue.

Our PC microcavity is an 11 (in Γ-M) by 21 (in Γ-K) array that has an internal pore wall surface area of ~ 50 μm^2. With the present device, we are capable of detecting a shift of ~ 0.1 nm. Thus the minimum amount of analyte that can be measured is 2.5 fg if we assume that the bio-molecules form a uniform monolayer on the internal surface of all the pores. The amount of analyte detected by our device is significantly reduced compared to SPR which requires a relatively larger sensing area (from 0.01 mm^2 to 1 mm^2 [20,21]). The performance of our biosensor can be further improved by optimizing the quality factor Q.

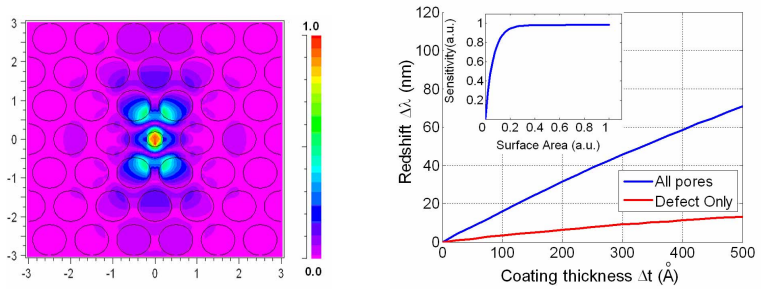

(a) (b)

Fig. 5. (a) Schematic of field confinement in a 2-D PC microcavity (the scales are in μm). The colorbar indicates the scale of electric field intensity. (b) Resonance redshift versus coating thickness on the pore walls. The blue curve shows the redshift due to the uniform infiltration of bio-molecules in all the pores. The red curve shows the redshift due to the infiltration only in the central defect. The inset at the top left shows the normalized sensitivity ($\Delta\lambda/\Delta t$) vs. the surface area covered by the bio-molecules. If the region coated with bio-molecules extends to pores away from the defect, the sensitivity first increases rapidly and then saturates.

As shown in Fig. 5(a), the electric field distribution is strongly localized in the defect which is the most sensitive region to a refractive index change. Thus, the contribution of the defect region should be larger than the rest of the pores. Fig. 5(b) demonstrates this by comparing the calculated amount of redshift due to the infiltration of bio-molecules in all the pores (blue curve) and that due to the infiltration only within the central defect (red curve). In the latter case, the sensitivity given by $\Delta\lambda/\Delta t$ drops by a factor of 4, however, the total amount of bio-molecules required decreases from 2.5 fg to 0.05 fg. Fig. 5(a) also shows that the electromagnetic field strength in neighboring pores is not completely negligible. If we increase the area covered by the bio-molecules from the central defect to surrounding pores located in increasingly large concentric circles, the sensitivity first increases but then saturates very rapidly. The Fig. inset plots the sensitivity, normalized to its maximum value obtained by coating uniformly in all the pores, versus the percentage of the total surface area that is covered by the bio-molecules.

#79144 - $15.00 USD Received 18 Jan 2007; revised 23 Mar 2007; accepted 23 Mar 2007; published 3 Apr 2007

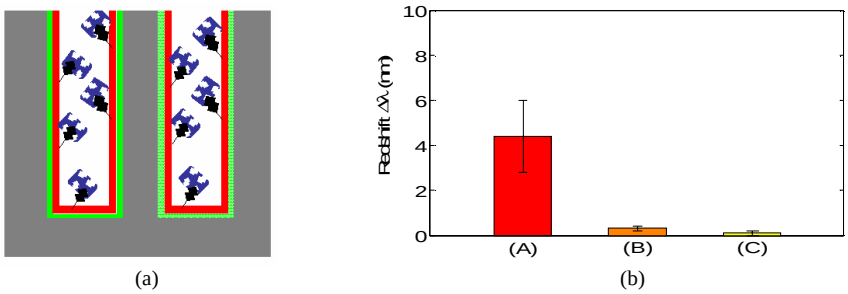

Fig. 6. (a) Schematic of biotin-streptavidin binding recognition. (b) Amount of resonance red-shift resulting from device exposure to different solutions. Bar (A) shows the amount of redshift resulting from specific binding of streptavidin to biotin. Bar (B) shows that the contribution to the shift from non-specific binding (no probe molecule) is negligible. Bar (C) shows that there is no contribution by the buffer alone.

Two important benchmarks for a biosensor are sensitivity and selectivity. Previous experiments demonstrate the capability of detecting the dehydrated protein layer thickness as thin as 1 Å. However glutaraldehyde-BSA binding is a non-specific binding process; thus, it only shows the presence of bio-molecules inside the microcavity without specifying the type of proteins. To demonstrate the selectivity of this device, we use biotin-streptavidin coupling as the model system. We first functionalize the device with the probe molecule (Sulfo-NHS-LC-LC-Biotin) which has an extremely high binding affinity for the target molecule (Streptavidin). Each streptavidin molecule has four equivalent sites for biotin which makes it an excellent molecular linker in many assays. As shown in Fig. 6(a), the target molecules are immobilized on the pore walls in the presence of the probe molecules. The experimental results shown in Fig. 6(b) demonstrate the selectivity of this biosensing platform as well as its ability to avoid false positive signals. Bar (A) shows that the specific binding of streptavidin to biotin introduces a ~ 4 nm redshift. Bar (B) shows that the contribution to the resonance shift from non-specific binding (no probe molecule) is negligible. Bar (C) shows that there is no contribution from the buffer alone.

In conclusion, we have demonstrated an ultra-sensitive biosensor that consists of a 2-D Si PCs microcavity. Binding of BSA to glutaraldehyde is monitored by measuring the spectral resonance redshift. This sensor can quantitively measure the dehydrated protein size. The present device can detect the presence of 2.5 fg of analyte. Its performance can be further improved by increasing the Q factor and positioning the biological substance in the defect region only. Experiments carried on specific biotin-streptavidin model indicate the selectivity of the device.

Acknowledgments

This work is supported by the National Science Foundation through grant BES 04279191. The devices are fabricated in part at the Cornell NanoScale Facility, which is supported by the National Science Foundation grant ECS 03-35765. The authors gratefully thank Dr. M. Haurylau, Dr. H. Ouyang and H. Yoo for helpful discussions.

#79144 - $15.00 USD Received 18 Jan 2007; revised 23 Mar 2007; accepted 23 Mar 2007; published 3 Apr 2007